Structural organization of the needle complex of the type III secretion apparatus of Shigella flexneri

Sani, Musa; Allaoui, Abdelmounaaïm; Fusetti, Fabrizia; Oostergetel, Gerrit; Keegstra, Wilko; Boekema, Egbert J.

Published in:
Micron

DOI:
10.1016/j.micron.2006.04.007

Available online at www.sciencedirect.com
ScienceDirect
Micron 38 (2007) 291–301
micron
www.elsevier.com/locate/micron

Structural organization of the needle complex of the type III secretion apparatus of *Shigella flexneri*

Musa Sani [a], Abdelmounaaïm Allaoui [b], Fabrizia Fusetti [c], Gert T. Oostergetel [a], Wilko Keegstra [a], Egbert J. Boekema [a,*]

[a] *Biophysical Chemistry, Groningen Biomolecular Sciences and Biotechnology Institute, University of Groningen, Nijenborgh 4, 9747 AG Groningen, The Netherlands*
[b] *Laboratoire de Bacteriologie Moleculaire, Faculté de Medecine, Université Libre deBruxelles, 808 Route de Lennik, CP 614 b, B-1070 Bruxelles, Belgium*
[c] *Biochemistry, Groningen Biomolecular Sciences and Biotechnology Institute, University of Groningen, Nijenborgh 4, 9747 AG Groningen, The Netherlands*

Received 28 February 2006; received in revised form 11 April 2006; accepted 11 April 2006

Abstract

The secretion apparatus known as the needle complex (NC) from the bacterium *Shigella flexneri* was studied by single particle electron microscopy. The isolated intact NC appears in projection to be composed of a basal body consisting of seven rings and a protruding needle appendage. A comparison of averaged projections of the intact NC and its fragments revealed the organization of the NC into several major subcomplexes. One of these lacks an inner membrane ring of the basal body but still presents the needle appendage attached to four upper rings. The position of the needle appendage within these rings is variable, suggesting that the dissociated component is necessary for stabilizing the needle appendage. Averaged images of the subcomplex lacking the inner membrane basal rings show a thicker extension at the base of the needle appendage, called the socket. This socket was also found to be present in images of the basal body fragment isolated from mutants lacking the *mxiH* and *mxiI* genes. This suggests that the socket is not composed of MxiH and MxiI subunits, which form the needle appendage. A symmetry analysis of the basal body top view projections indicated that a peripheral protein component of the inner membrane ring is present in a ring with 24 copies, in contrast to the *Salmonella typhimurium* NC. A model is presented in which the NC is only associated to the outer- and inner-membranes with its first and seventh ring, respectively.

Keywords: *Shigella flexneri*; Type III secretion system; Needle complex; Basal body; Electron microscopy

1. Introduction

Pathogenic bacteria have evolved a variety of delivery systems to translocate their proteins (some of them virulent in nature) to their host and/or surrounding environment. One such system, termed the type III secretion system (TTS), is used by pathogenic Gram-negative bacteria to cause a variety of diseases in animals and plants. The TTS is a supramolecular system used as a molecular syringe to inject proteins directly into host cells (Hueck, 1998). Characteristic features of this system are (i) the absence of a typical, cleavable, *sec*-dependent signal sequence in secreted substrates; (ii) the requirement of accessory proteins for secretion; (iii) the transit of proteins through both the inner and outer bacterial membranes; and (iv) the requirement of activating signals to initiate secretion. The TTS apparatus is a complex multi-subunit membrane-bound structure consisting of more than 20 proteins (Cornelis and Van Gijsegem, 2000). Approximately eight components of this apparatus are homologous to components of the flagellar assembly apparatus, indicating a common ancestry (Hueck, 1998). The bacterial effector molecules that transit through the secretion apparatus and their resulting effects on eukaryotic cells vary among different pathogens. Whereas *Shigella* and *Salmonella* deliver their effectors to facilitate their uptake by non-professional phagocytes, *Yersinia* spp. and enteropathogenic *Echerischia coli* deliver theirs to inhibit uptake by macrophages (Hueck, 1998).

Bacteria of the *Shigella* group are the causative agent of bacillary dysentery in humans (LaBrec et al., 1994). Bacteria

* Corresponding author. Tel.: +31 50 3634225; fax: +31 50 3634800.
E-mail address: e.j.boekema@rug.nl (E.J. Boekema).

0968-4328/$ – see front matter © 2006 Elsevier Ltd. All rights reserved.
doi:10.1016/j.micron.2006.04.007

are transmitted via the faecal-oral route and cause disease by invading the colonic epithelium, which results in tissue destruction and inflammation (LaBrec et al., 1994). Genes required for bacterial entry into host cells are clustered on a 30 kb region of the 220 kb virulence plasmid (Buchrieser et al., 2000) and encode a TTS apparatus and effectors that induce internalization of bacteria. The TTS apparatus (~50 copies per cell) is assembled at 37 °C before any host contact (Tamano et al., 2000).

Recent studies indicate that the needle complex (NC) of *Shigella* and *Salmonella* spp. share structural similarities, with a base embedded in the bacterial membrane and an axial structure protruding from the bacterial surface to form a needle-like rod (Tamano et al., 2000; Blocker et al., 1999; Kubori et al., 1998). Electron microscopy studies on the NC from *S. flexneri* and *Salmonella* spp. revealed that the NC is composed of a basal body which consists of pairs of upper and lower rings (Tamano et al., 2000; Kubori et al., 1998) and a tubular needle appendage of about 450–500 Å in length which protrudes from the basal body. The latter has a diameter of ~70 Å enclosing a central channel of about 25 Å and is composed of MxiH and MxiI in *S. flexneri* and of PrgI and PrgJ in *Salmonella*, of which MxiI and PrgJ are indicated to be minor essential components (Tamano et al., 2000; Blocker et al., 2001; Kimbrough and Miller, 2000; Kubori et al., 2000). The 3D structure of the needle appendage of the NC of *Shigella* was solved at a resolution of 16 Å and resembles the helical architecture seen in the flagellar hook and filament (Cordes et al., 2003). It is interesting to note that a complete atomic model of the flagellum obtained by cryo-electron microscopy and image analysis (Yonekura et al., 2003) shows that flagellin subunits are held together by hydrophobic interactions, and that the central channel of the flagellum is lined with polar residues.

The base structure of the NC is composed of three major components, MxiD, MxiG, and MxiJ in *S. flexneri* and InvG, PrgH, and PrgK in *S. typhimurium* and resembles the flagellar basal body (Tamano et al., 2000; Blocker et al., 1999; Kubori et al., 1998). These three major components of the base structure all have cleavable N-terminal *sec*-dependent export signals (Allaoui et al., 1992, 1993). While MxiG and MxiJ form most of the basal part (Blocker et al., 1999) MxiD has been proposed to form the upper ring doublet of the NC (Blocker et al., 1999). Detailed structural analysis of the basal part of the NC from *Salmonella typhimurium* has revealed that the basal part (which henceforth will be referred to as the basal body due to its structural similarity to the flagellar basal body) possesses a 20- or 21-fold symmetry in the inner ring (Marlovits et al., 2004).

In the present study, we have used electron microscopy and single particle analysis to get further insight into the structural assembly of the NC of *Shigella flexneri*. Purification of the NC was achieved by gel filtration and CsCl gradient centrifugation. This procedure yielded, in addition to many intact NCs, several intermediate subcomplexes, which were also analyzed. Additional information was obtained by a structural analysis of the basal body from mutants lacking specific subunits. Based on these data, the division of the NC into several distinct substructures is discussed.

2. Materials and methods

2.1. Bacterial strains and growth media

The *S. flexneri ipaC* strain SF621, a derivative of the wild-type strain M90T, serotype 5 (Menard et al., 1993), was a kind gift from Dr. C. Parsot (Pasteur Institute, Paris). This strain produces normal NC, but is non-invasive, due to the absence of the IpaC translocator. Other mutant strains used in this study are SB116 (relevant genotype *mxiH*$^{-}$) and SB125 (relevant genotype *mxiI*$^{-}$) (Blocker et al., 1999). Bacteria were grown in tryptic casein soy broth (Sigma) supplemented with kanamycin (30 μg ml^{-1}) at 37 °C.

2.2. Purification of NC and dissociation experiments

The needle complexes of *S. flexneri* were extensively purified from the envelope fractions by adaptation of the method described by Tamano et al. (2000). In brief, to allow spheroblast formation bacteria were suspended in 20% sucrose supplemented with 2 mM EDTA and 0.5 mg/ml lysozyme (Sigma). Cells were lysed with 0.1% Triton X 100 at a total protein to detergent ratio of 5:1 (w/w), followed by DNA digestion with 4 mM $MgCl_2$ and 80 μg/ml DNAse (Sigma). The membrane fraction was separated by ultracentrifugation at 110,000 × *g* for 1 h. The resulting pellet was resuspended in TET buffer (10 mM Tris–HCl, pH 8.0, 1 mM EDTA, 0.1% Triton X-100) and loaded onto a Superdex 200 gel filtration column (Amersham Biosciences) at a flow rate of 0.4 ml/min. Fractions containing the NC were collected and concentrated by centrifugation at 80,000 × *g* for 45 min, and subsequently resuspended in TET buffer. Column fractionated samples were further purified by 40% (w/v) CsCl density gradient centrifugation in a SW41 rotor at 37,000 × *g* for 14 h at 20 °C. To isolate NC components from *mxiH* and *mxiI* mutants, harvested cells were first cross-linked as previously described (Schuch and Maurelli, 2001). Membrane fractions were prepared and solubilized as described above for the *ipaC* mutant. The preparation was then loaded onto a Mono Q HR 5/5 column (Amersham Biosciences), which had been pre-equilibrated with five column volumes of TET buffer. Bound proteins were eluted with a linear gradient of 0–1 M NaCl, pH 8.0. Fractions were pooled and centrifuged at 250,000 × *g* for 1 h. The pellets were resuspended in TET buffer and analyzed by SDS/PAGE. Proteins were either transferred to a nitrocellulose membrane and immuno-blotted as previously described (Magdalena et al., 2002) or prepared for matrix-assisted laser desorption/ionization tandem mass spectrometry (MS/MS) analysis (MALDI-MS/MS).

2.3. MALDI-MS/MS analysis

Purified particles obtained from the IpaC, MxiH and MxiI deficient mutants were separated on a 15% (160 mm × 160 mm × 1.0 mm) tricine SDS-polyacrylamide gel and stained with colloidal Coomassie Blue (Serva). Each lane was systematically cut and excised gel fragments were washed for 1 h with

25 mM ammonium bicarbonate, 50% HPLC grade acetonitrile and further dehydrated in pure acetonitrile. Hundred nanograms trypsin (Sequencing grade modified, Promega) in 25 mM ammonium bicarbonate (pH 7.8) were added to each gel fragment. Digestion was carried out overnight at 37 °C. The resulting tryptic peptides were extracted twice with 0.1 ml of 60% (v/v) acetonitrile/1% (v/v) trifluoroacetic acid in an ultrasonic bath for 15 min. Extracts were pooled, lyophilized and the peptides dissolved in 10 μl 0.1% (v/v) trifluoroacetic acid. Peptide samples (0.5 μl) were mixed on the MALDI target with 0.5 μl of alpha-cyano-4-hydroxycinnamic acid, in 50% (v/v) acetonitrile/0.1% (v/v) trifluoroacetic acid, and left to dry. MALDI spectra were recorded on a MALDI TOF/TOF mass spectrometer 4700 Proteomics Analyzer (Applied Biosystem, Framingham, MA, USA). The most abundant peptides were subjected to MS/MS fragmentation. Data were analyzed using GPS Explorer software (Applied Biosystem). MSDB and Swiss-Prot database were searched with the MASCOT software (Matrix Science, London, UK). A tolerance of 0.15 Da for both the MS and MS/MS analyses, and one missed cleavage site were set as fixed parameters.

2.4. Electron microscopy and image analysis

Samples of purified complex were negatively stained using the droplet method with 2% uranyl acetate on glow discharged carbon-coated copper grids. Electron microscopy was performed on a Philips CM20FEG equipped with a field emission gun operated at 200 kV. The ''GRACE'' system for semi-automated specimen selection and data acquisition (Oostergetel et al., 1998) was used to record 2048 × 2048 pixel images at 66,850× calibrated magnification with a Gatan 4000 SP 4K slow-scan CCD camera. The step size (after binning the images) was 30 μm, corresponding to a pixel size of 4.5 Å at the specimen level. A total of 10,000 particle projections were collected interactively from 3500 images. Single particle analysis was performed as previously described (Harauz et al., 1988) with IMAGIC and Groningen Image Processing (''GRIP'') software packages (W. Keegstra, unpublished data) on a PC cluster. Briefly, the images were first treated to normalize the variance and band-pass filtered to remove unwanted high and low frequencies of the images during the analysis. Projections were subjected to rotational and translational alignments with correlation methods (Harauz et al., 1988; Van Heel et al., 1992). The aligned projections were treated with multivariate statistical analysis (MSA) in combination with hierarchical classification (Van Heel et al., 1992). During classification, 15–20% of the images was rejected. Finally, sums of projections belonging to the various classes were made by adding the original images without imposed band-pass filter. The best 60–80% of the class members was taken for the final sums using the correlation coefficient of the alignment procedure as the quality criterion. The resolution of the class averages was calculated by Fourier ring correlation using the 3σ criterion (Van Heel, 1984). In addition, two subsets were independently processed in parallel by reference-free alignment procedures (Penczek et al., 1992) for comparison. The resolution of the class averages was estimated from the latter by Fourier ring correlation using the 3σ criterion (Van Heel, 1984).

To precisely localize the positions of substructures within the NC, difference mapping of averaged projections was performed. In this approach, normalized class sum images representing side-view projections of the NC and subcomplexes were subtracted from one another. Positive differences appear in white, negative differences in black and insignificant differences in gray. Rotational symmetry analysis of top views was performed according to Kocsis et al. (1995). In brief, 95 top views of the basal body from a mutant preparation were centered to a reference obtained by averaging the data set after translational alignments. By comparing the rotational power spectrum of centered particles with background images picked from individual micrographs, signals that are marginally above the background will build up to a statistically significant level to give the rotational symmetry.

3. Results

3.1. Purification of NC and electron microscopy

To investigate the structure of the needle complex (NC), single particles of the complex were isolated from three different mutants of *S. flexneri*. Intact NCs were purified from SF621 *ipaC*. This strain produces normal NCs, but is non-invasive, due to the absence of the IpaC translocator (Menard et al., 1993). Solubilized membrane fractions were first loaded onto a size exclusion column to separate the NC components from large membrane fragments (Fig. 1A). Aliquots containing NC components (checked by EM) were pooled and concentrated and further fractionated by 30% (w/v) CsCl density gradient centrifugation. In this way, a relative high number of pure intact complexes could be obtained (first lane of Fig. 1B). Resolved proteins in Fig. 1B were subjected to in-gel trypsin digestion followed by MALDI-MS/MS analysis. The results clearly show the presence of MxiD, MxiG, MxiJ and MxiM subunits in all three samples, while MxiH is only detected in the NC components expressed by the *ipaC* mutant (Fig. 1B). MxiM is observed to co-purify with all NC components isolated from all the investigated strains and thus indicates that it associates with the isolated complex. Neither in *Shigella* (Tamano et al., 2000; Blocker et al., 1999) nor in *Salmonella* (Marlovits et al., 2004) has this subunit been detected in previous isolations of this complex. Similar sample compositions were detected by MS analysis irrespective of whether the particles were isolated by CsCl gradient centrifugation or by size-exclusion chromatography (data not shown), and thus rules out that the observed components could be due to artifacts. The fraction from the *ipaC* mutant of Fig. 1B showed, besides the relatively homogeneous monodisperse NC particles, also particles of NC-like substructures. Apparently, the purification step resulted in a limited dissociation of the NC. This dissociation is corroborated by Fig. 2 where three types of subcomplexes are visible, which were tentatively classified as: (i) NCs minus the needle appendage denoted as BB (for basal body); (ii) NCs lacking the inner

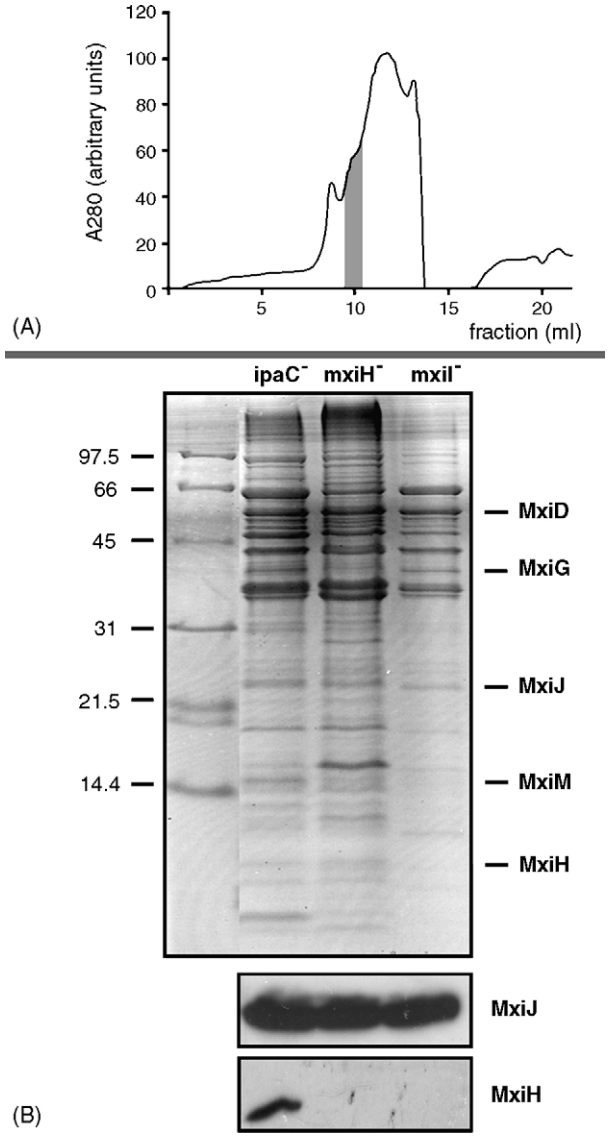

Fig. 1. (A) Gel chromatography of solubilized needle complexes. The fraction containing the highest numbers of NCs (as checked by EM), used for further purification with density gradient centrifugation, is indicated. (B) Tricine SDS-PAGE of purified NC and its subcomplexes *S. flexneri* mutant strains. Samples from the three different strains (IpaC$^-$, MxiH$^-$, MxiI$^-$) were separated on a 15% gel stained with colloidal Coomassie Blue stain (upper part) or blotted with antibodies specific for MxiJ and MxiH (lower part).

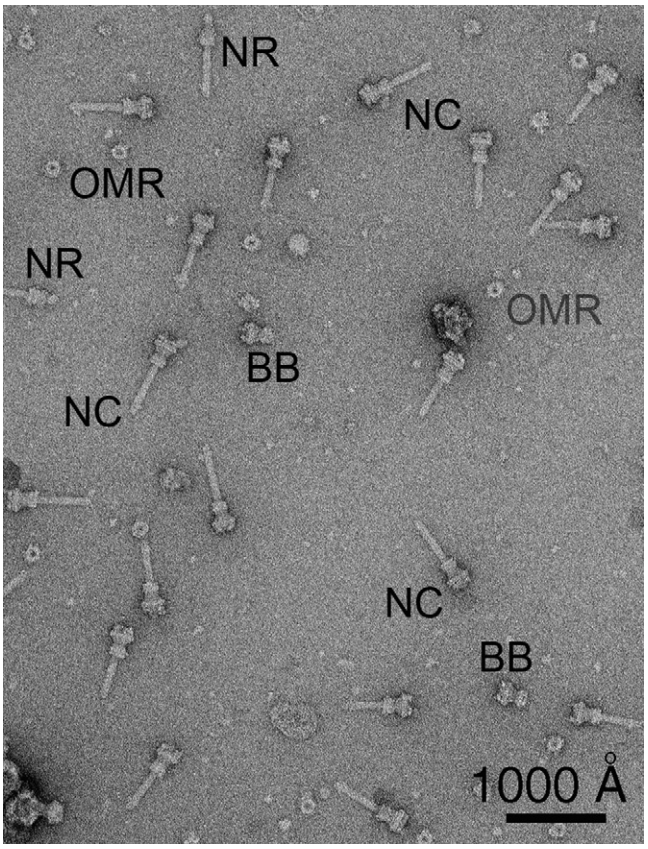

Fig. 2. An electron micrograph of negatively stained purified NC particles isolated from an IpaC$^-$ strain after the CsCl gradient step. Some complete NCs have been indicated (NC). Three specific fragments are dominant: first, so-called basal bodies which are NCs lacking the needle appendage (BB); second, NCs lacking the inner membrane rings (NR) and third, dissected outer membrane rings (OMR).

membrane rings denoted as NR (for needle plus rings) and (iii) an outer membrane ring subcomplex, denoted as OMR. The population of all three subcomplexes was relatively homogeneous. No continuum of intermediate subcomplexes was found, suggesting that the dissociation of the NCs is stepwise.

We also investigated NC components from two *S. flexneri* mutants deficient either in MxiH or MxiI. These proteins are proposed to be the sole components of the needle appendage of the NC (Tamano et al., 2000; Blocker et al., 1999; Kubori et al., 1998). NCs lacking the needle appendage were purified from both MxiH and MxiI deficient strains. Samples purified from both mutant strains were analyzed by MALDI-MS/MS. MxiD, MxiG, MxiJ and MxiM were identified (Fig. 1B), but not MxiH and MxiI. This is consistent with previous observations (Blocker et al., 1999). Western immuno-blotting confirmed the presence of MxiH (Fig. 1C) and MxiI (data not shown) only in the *ipaC* mutant. In contrast, MxiH could not be detected in *mxiI* mutant preparations; conversely, MxiI was also not detected in *mxiH* mutant preparations (data not shown), a finding consistent with earlier observations (Sukhan et al., 2003).

3.2. Image analysis

Single particle image analysis was performed by selecting all well-preserved projections from non-overlapping NC particles and subcomplexes from a large set of electron microscopy images. Over 10,000 particles were picked from the *ipaC* mutant strain, of which 66% were intact NCs, while the remaining projections were assigned to the OMR subcomplex (17%), the NR (9%), and basal body (8%), respectively. With the exception of the OMR projections, which were assumed to represent a top view orientation, the NC particles and the remaining subcomplexes all oriented on the carbon film in a side view position approximately perpendicular to the long axis of the complex. In an initial alignment step, one projection was selected arbitrarily

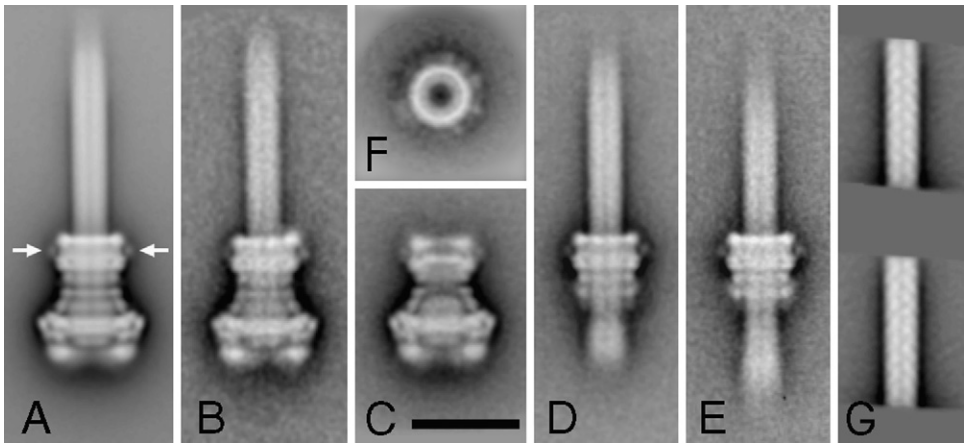

Fig. 3. Image analysis of the whole NC and four specific subcomplexes of the ipaC mutant. A set of 8250 projections represents the most abundant projections of five different types of (sub)complexes that were independently processed after sorting out by an initial classification. The final projections represent averages of the best classes with (A) a sum of 1500 needle complex particles showing strong mirror-symmetry along the vertical axis within the basal body part. White arrows indicate prominent spikes between the upper two rings of the basal body part; (B) subset of 63 needle complex particles without strong mirror symmetry, as can be seen from the upper ring of the basal body and protrusions, of which only the one at the right of the basal body is visible; (C) 337 basal body particles; (D) 343 NR particles; (E) 243 NR particles and (F) 450 OMR particles. (G) Result of classification (2 classes of 1536 projections each) of needle appendages from needle complex particles, which were aligned after masking the basal body moiety. The space bar indicates 250 Å.

from the set of images and used as a first reference. After the first alignment relative to this noisy image, a new reference was generated by summation of the images with the highest correlation coefficient related to the first reference. The aligned data set was treated by MSA and partitioned into 113 classes. It was subsequently reclassified into five major classes representing the different particle types. These classes were further partitioned into several classes by independent MSA and hierarchical classification procedures to determine inter-class difference. The quality of these average classes was further improved by iterative alignments in a multi-reference alignment scheme. Fig. 3 shows the final averaged projections of the five particle types. The reproducibility of the features in the average was assessed by independently analyzing subsets of projections obtained from different preparations by a reference free alignment procedure (Penczek et al., 1992). Specific features visible in these particle types are discussed below.

3.3. Needle complex

A total of 4158 whole NC particles, composed of a needle appendage protruding from a basal part composed of several rings was analyzed. Alignment was carried out with respect to the basal part of the complex since the overall length of the needle appendage is somewhat variable. The classification of this data set showed only one dominant view (Fig. 3A). In this view the basal part with a height of 310 Å is clearly resolved. The resolution of this component in the final average projection was estimated to be 16 Å using the 3σ criterion (Van Heel, 1987) and 19 Å using the 0.5σ criterion. Characteristic features of this projection are protrusions attached to the periphery of the OMR doublet (see arrows in Fig. 3A). This density protrudes about 25 Å from the ring doublet and is located right within the OMR. It is surprising that only one type of dominant projection was found for the whole NC particles. We only found a very limited number of projections that deviated from this dominant view of Fig. 3A if the aligned set was decomposed into about 100 classes (Fig. 3B). It shows an average image with some deviations around the upper two rings of the basal part. Moreover, only the protrusion on the right side is clearly visible.

The needle appendage of the NC is a straight hollow tube (indicated by a stain penetrated line along its axis) which is 500 Å long on average. The overall size and shape of the NC are in agreement with previous investigations (Tamano et al., 2000; Blocker et al., 1999; Kubori et al., 1998; Cordes et al., 2003). However, details in the needle portion appeared to have been smeared out during averaging procedures. Significant features of the needle portion could be resolved when projections were aligned and classified after masking the basal part. A decomposition into two classes, each of 1536 projections is shown in Fig. 3G.

3.4. The basal body

A subset of 701 side views of basal body (BB) particles isolated from the *ipaC* mutant strain was processed and one dominant projection was obtained (Fig. 3C). Similar BBs could also be obtained from the MxiH and MxiI deficient strains. Actually this was the only intact components that could be purified from these mutants. The micrographs of EM samples prepared from both *mxiH* and *mxiI* mutants, however, showed low numbers of such particles per image. The number of particles increased slightly when a cross-linking step was included in the isolation procedure. A total of 500 particles could be picked from more than 2000 images. Average projections of side views of these mutants show a basal body lacking the needle appendage (Fig. 4A and B), identical to the substructure co-purified from the *IpaC* mutant (Fig. 4C). A striking feature of all three basal body projections is the presence of a central oval-shaped ‘‘bulge’’ in the lower half of the particle. This feature was described as a

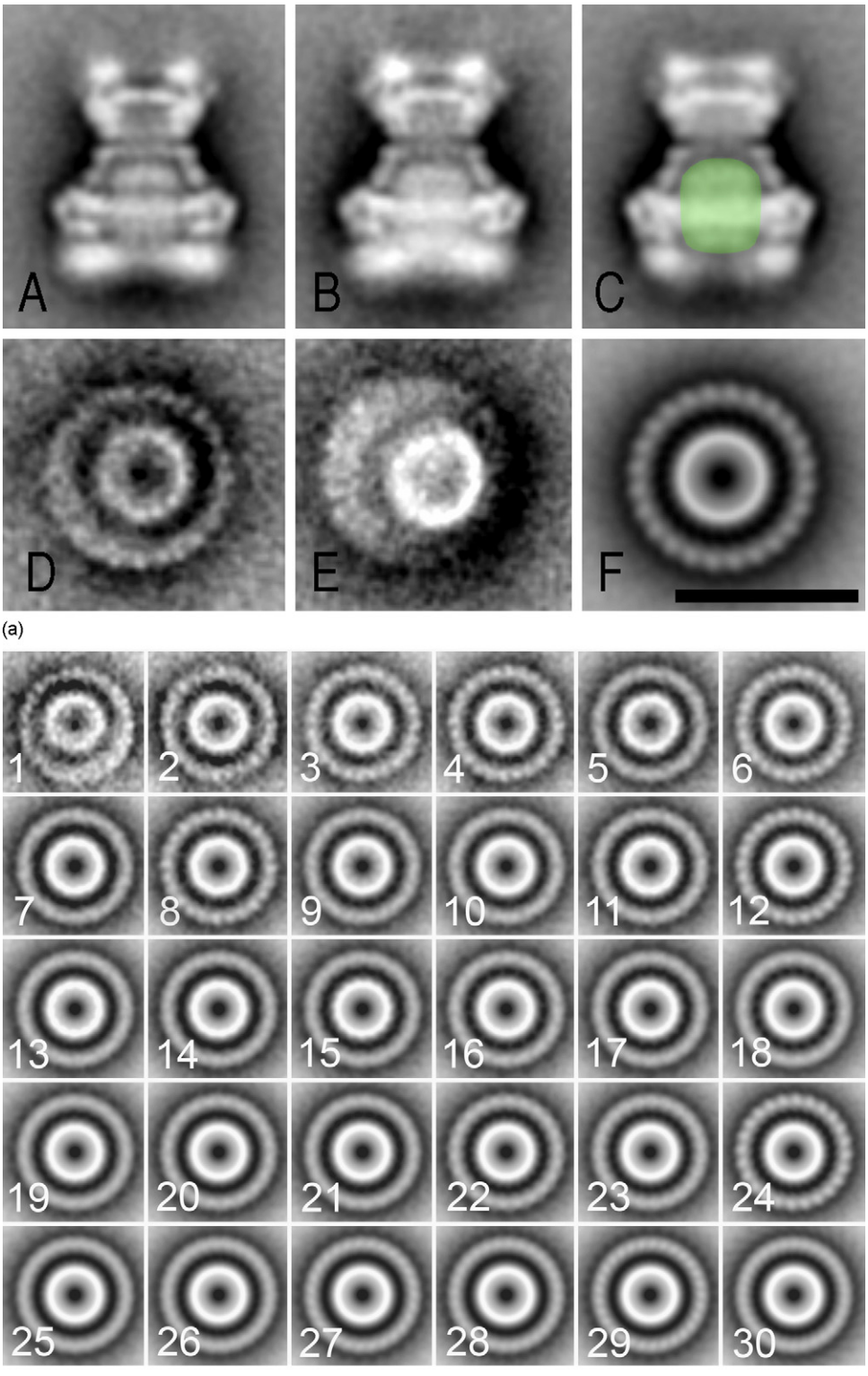

Fig. 4. (A–C) Averages of side view projections of the basal body isolated from mutants of MxiH, MxiI and ipaC, respectively. The ''socket'' has been indicated in the frame of (C), (the same as frame Fig. 3C), by a green overlay. (D–E) Averages of top view projections of basal body of mutants of *mxiH* and *mxiI*, in which the particles are tilted slightly out of plane. (F) The top view of the basal body of the *mxiH* mutant, with 24-fold symmetry imposed. Lower half: symmerty analysis of the image of frame D. The *n*-fold type of rotational imposed on frame D has been indicated. The sacle bar in A–F indicates 250 Å.

socket in a 17 Å 3D reconstruction of the type III secretion complex from *S. typhimurium* (Marlovits et al., 2004) and hence this name will be kept up. In addition to the observation of side views of basal bodies lacking the needle appendage, we also observed top view projections. Examination of the average top view from the *mxiH* and *mxiI* mutants show small densities arranged in an inner ring of 90 Å and an outer ring of 246 Å (Fig. 4D and E). It is reasonable to infer that these densities correspond to individual subunits that arrange to form these annular substructures. A symmetry analysis of the basal body top views of the *mxiH* mutant was performed. By comparing 2–30-fold imposed rotational symmetries it is apparent that the outer ring of densities has a clear 24-fold rotational symmetry, as well as the lower 2-, 3-, 6-, 8- and 12-fold symmetries and that all other imposed types of rotational symmetries did not enhance the image features (Fig. 4, lower half). Therefore, the 24-fold rotational symmetry was imposed in Fig. 4F. No such periodicity is observed for the inner ring suggesting that the inner ring has a different symmetry; which is possibly 15-fold (Fig. 4, lower half). The view of the *mxiI* mutant is too far tilted out of the horizontal plane to determine its rotational symmetry.

The resolution attained for all three basal body side view averages is 19 Å. The lower part of the basal body has an overall dimensions of 310 Å (height) × 242 Å (diameter), while the upper rings which might be inserted in the outer membrane and the peptidoglycan layer have a height of 81 Å and a diameter of 158 Å. Immediately below the outer membrane ring (OMR) doublet are three minor rings with diameters of 122, 135 and 161 Å. At the base is an inner membrane ring with a diameter of 240 Å and a height of 58 Å. Comparison of the basal body fragments from the *ipaC* mutant with those isolated from *mxiH* and *mxiI* mutants shows no discernible differences suggesting that the basal body which co-purified with intact NC could be an intermediate substructure before the polymerization of the needle portion occurs.

To characterize the extent of the needle insertion into the BB, difference mapping between intact NC (Fig. 5A) and the mutants was performed (Fig. 5B). Since the immunoblot analysis of both mutants shows the absence of both MxiH and MxiI in either mutants (Fig. 1), the positive density observed for the needle appendage is of a substructure solely composed of MxiH and MxiI (which is present in the intact NC preparation).

3.5. Outer membrane ring

A total of 1433 particle projections with a ring-shaped form was analyzed. After repeated cycles of alignments and classification the averaged projection of the major classes shows a ring with an outer diameter of 157 Å and a sharply defined central cavity with a radius of 76 Å (Fig. 3F). The rings are assigned to the outer membrane ring (OMR) substructure. These rings have diameter and pore size consistent with OMR classifications (Bitter, 2003; Sukhan et al., 2001) and thus are likely to be composed of MxiD subunits (see Section 4). Another reason for the assignment is the presence of spikes at the periphery of the rings (Fig. 3F), which likely correspond to the extensions observed in the OMR part of the whole NC projection (Fig. 3A). Although they appear in angular periodicities, the precise number of spikes could not be established with certainty, due to the low number of projections (below 50) with a complete set of spikes.

3.6. The needle appendage

Statistical analysis and classification of the subset of 742 images of the needle complex lacking the lower basal rings

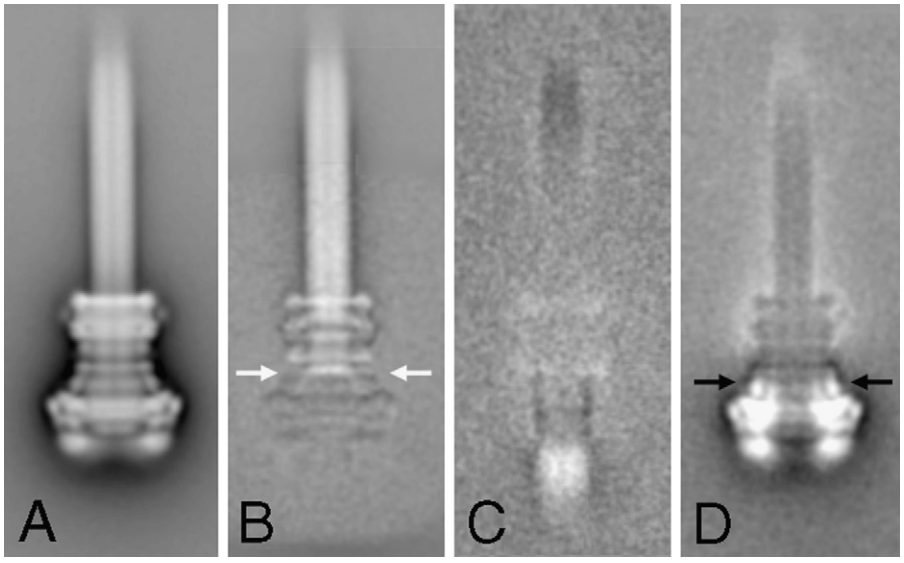

Fig. 5. Comparison of NC components by difference mapping. (A) Average projection of intact NC from 3A. (B) Difference image of 5A minus 4A shows the extent of the needle extension into the basal body (BB); the diameter of the needle narrows as the needle inserts into the BB. (C) Difference image of 3E minus 3D shows positive densities confirming a downward shift of the needle. (D) Difference image of 3A minus 3D shows dissociated fragments of the inner membrane rings of the BB (black arrows; Fig. 5D). Strong positive (white) densities represent protein components that disappeared during needle dissociation from the complete NC. White arrows indicate to which extent the needle appendage is inserted into the BB.

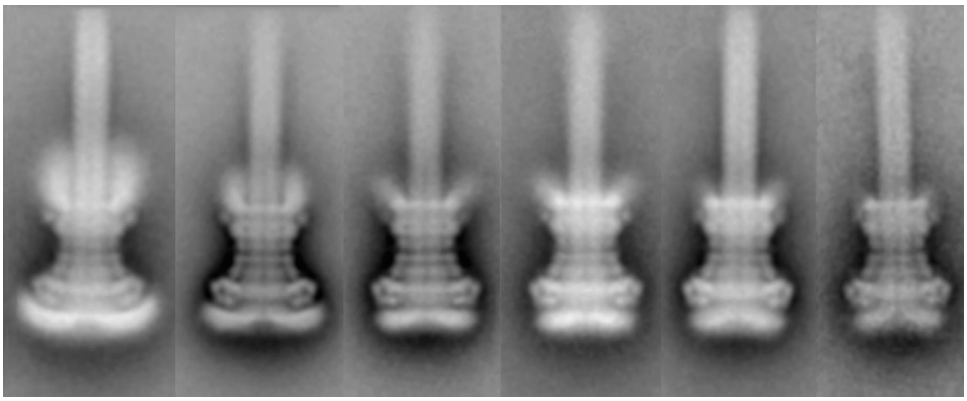

Fig. 6. Averaged images of side view projections of intact needle complexes isolated from the ipaC mutant with six different Triton X-100 concentrations. For each projection map, about 300 images were summed, on average. The Triton X-100 concentrations which were used from left to right: 0.01%, 0.05%, 0.25%, 0.5%, 1% and 2%, respectively.

revealed that all projections of this NR subcomplex show a needle appendage with a socket surrounded by the OMR and two of the minor rings. The largest variation present in the subset was the relative position of the needle appendage to the rings. Two main positions of the rings appeared to be dominant, although intermediates were also observed. Due to the rather limited size of the subset, the set was decomposed into two classes (Fig. 3D and E). The variability in length of the part of the needle appendage that was located either above or below the surrounding rings is obvious: one class shows a longer protrusion below the rings as compared to the other (Fig. 3D and E), though the average overall length of the needle appendage plus the socket remains constant. This is also clear from difference mapping between the two classes of Fig. 3E and D; the positive density at the lower base is compensated with the negative density at the upper tip (Fig. 5C). Difference mapping between the intact NC of Fig. 3A and the NRs subcomplex indicates that the loss of the inner membrane ring coincides with a dissociation of the lowest of the minor rings (black arrows; Fig. 5D).

3.7. Positioning of the NC with respect to the inner and outer membranes

Because the single particle electron microscopy as described above preferentially is performed on purified complexes, the NCs had to be disrupted from the membranes during purification. Hence, the position of the NC within the inner and outer membranes is not known. However, we found by checking with electron microscopy that the NCs already detach from the membranes after incubation with relatively low concentrations of the detergent Triton X-100. This detergent is able to release the NC even at concentrations below its critical micellar concentration (CMC), which is ∼0.02%, probably because only a small part of its total surface is hydrophobic. It is by definition not possible that Triton X-100 molecules will fully replace the lipids around the NC at concentrations below the CMC and hence it can be expected that remnants of the inner and outer membrane could be still attached to the NC depending on the concentration used during solubilization. We performed purifications of the NC at six different Triton X-100 concentrations in the range of 0.01–2% and averaged about 300 particle projections for each of the applied concentrations. It can be seen from Fig. 6 that the projection maps of the basal bodies are highly similar for all six purifications, except for the lowest and uppermost parts. They appear to become gradually thicker at decreasing detergent concentration. Since the negative stain does not penetrate lipid layers a shell of extra lipid molecules (plus some detergent) should be responsible for the increased thickness.

4. Discussion

To understand the morphology and organization of the NC of the TTS apparatus of *S. flexneri*, we examined complete NC and subcomplexes obtained by chromatography and density centrifugation by electron microscopy. Image analysis indicated that at the current resolution of 16 Å only one dominant type of projection of the complete NC was visualized (Fig. 3A), in which the left and right side of the BB part are remarkably similar. Differences only appear in a small number of projections (Fig. 3B). The fact that only one view was found is remarkable because usually at least slight differences in projections are found by single particle averaging due to roughness of the carbon support film which leads to differences in tilt. The dominant view can be explained if we assume that each of the rings of the BB consist of multiple copies of similar or identical domains, the appearance of just one dominant view may be caused by the fact that BB has some high-order symmetry. We determined that the peripheral component of the inner ring of the BB has a 24-fold rotational symmetry. Because of this symmetry the NC particles seemingly orient all in a very similar way on the support film with respect to the BB part. Interestingly, a symmetry of either 20 or 21 was determined for the inner ring component of the NC from *S. typhimurium* (Marlovits et al., 2004) indicating that the *Shigella* and *Salmonella* NCs are not identical.

The needle is built up by the polymerization of MxiH subunits. The final assembly results in a hollow tube of helically packed proteins with a constant diameter of 76 Å and a length confined to a narrow range of 450–500 Å. The recent 3D model

of the helical arrangement of the MxiH needle appendage (Cordes et al., 2003) shows about 5.6 subunits in one turn, with a helical pitch of 24 Å. The dominant projection of the whole NC does not show any detail in the needle portion (Fig. 3A). This was also the case when the aligned data set (aligned on the basal body) was classified only on the needle portion with decomposition into 100 classes. When the basal part is masked off and alignment performed with respect to the needle portion, features similar to helical turns as presented in the 3D model of Cordes et al. (2003) can be discerned (Fig. 3G). This may indicate that the needle does not have a fixed rotational orientation towards the basal body or a different symmetry.

Analysis of NR subcomplexes missing the inner membrane basal rings (IMR), shows a needle appendage with the OMR and two minor lower rings attached to it (Fig. 3D and E). Classification indicated a variable position of the needle appendage within the rings (Fig. 5C). This indicates that the needle appendage is not rigidly fixed to the OMR but is flexible in the absence of the IMR. Apparently the latter ring has a function in keeping the needle appendage in proper position. Because of its helical architecture, the needle diameter should be constant over its full length. However, the averaged projections of the NR subcomplexes, which are missing the major inner membrane rings (Fig. 3D and E), show a slight widening of the basal end of the needle. This widening is also obvious in many of the individual projections and is referred to as the socket (see Section 3).

Analysis of the basal body subcomplex indicates that this structure is composed of the same number of rings as in the complete NC. The averaged projection of the BB subcomplex in Fig. 4 shows a striking resemblance of these subcomplexes to the flagellar basal body (Francis et al., 1994; Sosinsky et al., 1992; Thomas et al., 2001). All three BBs contain the socket which directly confirms that this density is not part of the needle appendage. Comparison between BBs co-purified with intact NC and BB of *mxiH* and *mxiI* mutants show no discernible difference. This suggests that the BB isolated in intact preparation is an intermediate substructure of the NC. Although the basal bodies of the *mxiH* and *mxiI* mutants showed similar sockets as observed in the *ipaC* mutant, these mutants are not able to assemble a complete NC with a needle appendage. Since this needle appendage is composed of MxiH and MxiI, the socket should have a different protein composition.

The numerous ring-shaped projections (Fig. 3F) found in the data set represent a NC subcomplex which can only be assigned to the outer membrane ring (OMR) subcomplex, according to their diameter of 157 Å. The OMR substructure is probably composed mostly of MxiD, which is a member of the secretin superfamily (Allaoui et al., 1993). These proteins organize into multimeric ring-shaped structures. The stability of these structures is influenced by another protein, MxiM (Schuch and Maurelli, 1999). MxiM is a lipoprotein that belongs to a group of proteins called secretin pilots (Allaoui et al., 1992; Schuch and Maurelli, 1999). These proteins protect secretins from proteolysis in the periplasm and promote their insertion into the outer membrane by using their lipid extension to anchor this otherwise hydrophilic protein in the outer membrane (Schuch and Maurelli, 1999; Hardie et al., 1996). The average image of the OMR subcomplex suggests the presence of about 10 spikes (Fig. 3F), although the exact number of spikes could not be established due to the lack of a sufficient number of intact particles. These spikes are quite similar to those observed for the PulD–PulS complex (Nouwen et al., 1999), which suggests that they correspond to MxiM, the proposed functional equivalent of PulS. This is in agreement with previous studies that showed that MxiM and MxiD interact directly within the outer membrane envelope and co-purify together when co-expressed in *E. coli*. Similar spikes are also visible at the periphery of the averaged projection of complete NC (arrows, Fig. 3A). They protrude about 25 Å from the ring doublet and were not clearly resolved in previous studies (Blocker et al., 1999; Marlovits et al., 2004).

A comparison of subcomplexes of the NC could shed some light on the complicated composition of the type III needle complex, because the integrity of a particular substructure reflects the interaction of the individual components that make up that subcomplex. The present EM data on the subcomplexes can also be tentatively interpreted in the light of available biochemical data and a recent 3D model for the NC complex of *S. typhimurium* (Marlovits et al., 2004). We propose a model for the structural organization of the *S. flexneri* NC with seven protein rings in Fig. 7. The model presents for the first time the position of the inner and outer membrane, which appears to be almost exclusively associated with the first and last rings of the NC. In our model the NC is composed of seven rings of proteins, of which six are clearly visible in the projection maps of the intact NC. The upper four plus rings (in red) are present in the NR subcomplex of Fig. 3D and E and consist of two outer membrane rings and two minor rings, although actually only the upper of the two outer membrane rings is really associated to the outer membrane. In this subcomplex remnants of a fifth (minor) ring (in purple) are at the lower end of this complex. Hence, we consider the upper four rings to have strong interaction with each other. The upper two rings correspond to the OMR and probably contain the MxiD secretin. The spikes (orange) that protrude from the OMR would correspond to the MxiM secretin protein. This hypothesis is supported by the recent crystal structure of MxiM (Lario et al., 2005) that shows it as a conically shaped structure with dimensions of 40 Å × 30 Å × 30 Å. These spikes were not visible in the model of *Salmonella* (Marlovits et al., 2004). The third and fourth ring might correspond to either another portion of MxiD, possibly the N-terminal portion (Bitter, 2003) or MxiJ (Schuch and Maurelli, 2001).

According to the EM data the NC has a wider sixth ring which is embedded in the inner membrane (in blue). It should contain MxiJ, because it has a strongly hydrophobic region near its C-terminal extremity, which is proposed to span the inner membrane (Seydel et al., 1999; Yamaguchi et al., 1998; Yip et al., 2005). A recent crystal map of EscJ, which is a MxiJ homolog in enteropathogenic *E. coli* that lacks the C-terminal extremity (Yip et al., 2005), indicates that this protein could oligomerize to form a ring with 24 copies that is anchored to the inner membrane. MxiG has a strong hydrophobic central region

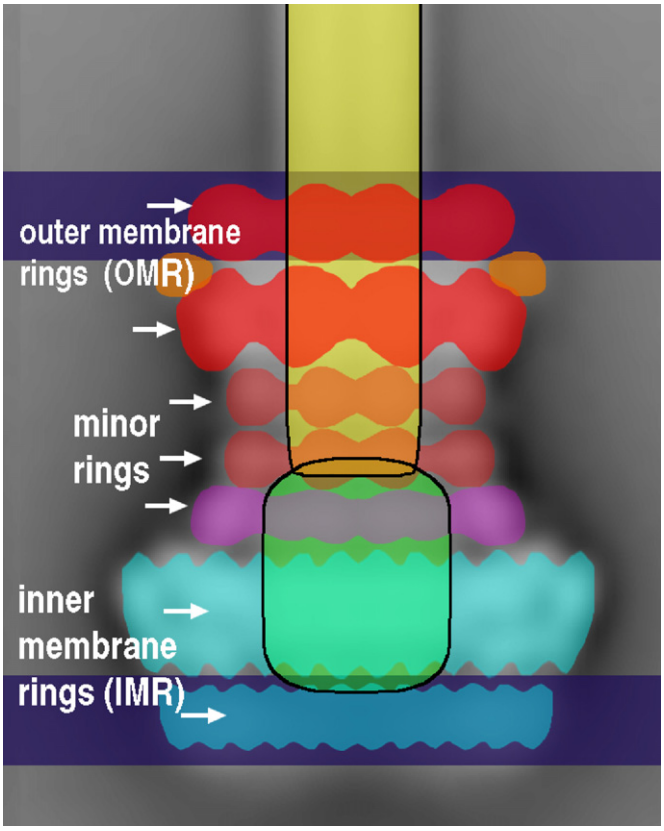

Fig. 7. Model for the position of components of the needle complex from *S. flexneri*. Components are color labeled as follows: the needle portion composed of MxiH and MxiI (yellow), the outer membrane ring (OMR) substructure mostly composed of MxiD and its periplasmic extension plus two additional minor rings (red) and MxiM spikes (orange). The MxiD periplasmic portion reaches towards and interacts with another minor ring assigned to MxiJ (purple). The two lower rings (blue) form the inner membrane rings (IMR) and appear to have a larger diameter than the upper four rings. The blue and purple rings thus facilitate space for the socket (green) which is attached to the lower end of the needle appendage. The inner and outer membranes have been indicated in purple. The symmetry of a peripheral IMR protein component was established to be 24; the symmetry of the components of the upper rings is not clear.

that is presumably inserted within the inner membrane as well (Allaoui et al., 1995) and thus should be a component of the inner membrane rings (IMR). Accordingly, its N-terminal domain should be located in the cytoplasm and its C-terminal domain in the periplasm, where it could interact with MxiD and/or MxiM (Blocker et al., 1999). The NC ends in our projection maps into two fuzzy globular masses of about 70 Å × 50 Å, which could represent a discontinuous ring (Fig. 3A). However, the 3D reconstruction from the *Salmonella* NC suggests that this is a very symmetrical continuous ring as well (Marlovits et al., 2004), bringing up the total number of rings up to 7.

Acknowledgements

We thank Dr. C. Parsot from the Pasteur Institute Paris and Dr. B.W. Dijkstra and Dr. C. Hamiaux from the Biophysical Chemistry Department of the University of Groningen for helpful discussions. We further thank Mrs. N. Bolaky for technical support.

References

Allaoui, A., Sansonetti, P.J., Parsot, C., 1992. *MxiJ*, a lipoprotein involved in secretion of Shigella Ipa Invasins, is homologous to *Yscj*. a secretion factor of the *Yersinia* Yop proteins. J. Bacteriol. 174, 7661–7669.

Allaoui, A., Sansonetti, P.J., Parsot, C., 1993. *MxiD*, an outer-membrane protein necessary for the secretion of the *Shigella Flexneri* Ipa Invasins. Mol. Microbiol. 7, 9–68.

Allaoui, A., Sansonetti, P.J., Menard, R., Barzu, S., Mounier, J., Phalipon, A., Parsot, C., 1995. *MxiG*, a membrane-protein required for secretion of *Shigella* Spp. Ipa Invasins—involvement in entry into epithelial-cells and in intercellular dissemination. Mol. Microbiol. 17, 461–470.

Bitter, W., 2003. Secretins of *Pseudomonas aeruginosa*: large holes in the outer membrane. Arch. Microbiol. 179, 307–314.

Blocker, A., Gounon, P., Larquet, E., Niebuhr, K., Cabiaux, V., Parsot, C., Sansonetti, P., 1999. The tripartite type III secreton of *Shigella flexneri* inserts *IpaB* and *IpaC* into host membranes. J. Cell Biol. 147, 683–693.

Blocker, A., Jouihri, N., Larquet, E., Gounon, P., Ebel, F., Parsot, C., Sansonetti, P., Allaoui, A., 2001. Structure and composition of the *Shigella flexneri* 'needle complex', a part of its type III secreton. Mol. Microbiol. 39, 652–663.

Buchrieser, C., Glaser, P., Rusniok, C., Nedjari, H., d'Hauteville, H., Kunst, F., Sansonetti, P., Parsot, C., 2000. The virulence plasmid pWR100 and the repertoire of proteins secreted by the type III secretion apparatus of *Shigella flexneri*. Mol. Microbiol. 38, 760–771.

Cordes, F.S., Komoriya, K., Larquet, E., Yang, S.X., Egelman, E.H., Blocker, A., Lea, S.M., 2003. Helical structure of the needle of the type III secretion system of *Shigella flexneri*. J. Biol. Chem. 278, 17103–17107.

Cornelis, G.R., Van Gijsegem, F., 2000. Assembly and function of type III secretory systems. Annu. Rev. Microbiol. 54, 735–774.

Francis, N.R., Sosinsky, G.E., Thomas, D., DeRosier, D.J., 1994. Isolation, characterization and structure of bacterial flagellar motors containing the switch complex. J. Mol. Biol. 235, 1261–1270.

Harauz, G., Boekema, E., van Heel, M., 1988. Statistical image analysis of electron micrographs of ribosomal subunits. Methods Enzymol. 164, 35–49.

Hardie, K.R., Seydel, A., Guilvout, I., Pugsley, A.P., 1996. The secretin specific, chaperone-like protein of the general secretory path-way: separation of proteolytic protection and piloting functions. Mol. Microbiol. 22, 967–976.

Hueck, C.J., 1998. Type III protein secretion systems in bacterial pathogens of animals and plants. Microbiol. Mol. Biol. Rev. 62, 379–433.

Kimbrough, T.G., Miller, S.I., 2000. Contribution of *Salmonella typhimurium* type III secretion components to needle complex formation. Proc. Natl. Acad. Sci. U.S.A. 97, 11008–11013.

Kocsis, E., Cerritelli, M.E., Trus, B.L., Cheng, N., Steven, A.C., 1995. Improved methods for determination of rotational symmetries in macromolecules. Ultramicroscopy 60, 219–228.

Kubori, T., Matsushima, Y., Nakamura, D., Uralil, J., Lara-Tejero, M., Sukhan, A., Galan, J.E., Aizawa, S., 1998. Supramolecular structure of the *Salmonella typhimurium* type III protein secretion system. Science 280, 602–605.

Kubori, T., Sukhan, A., Aizawa, S.I., Galan, J.E., 2000. Molecular characterization and assembly of the needle complex of the *Salmonella typhimurium* type III protein secretion system. Proc. Natl. Acad. Sci. U.S.A. 97, 10225–10230.

LaBrec, E.H., Schneider, H., Magnani, T.J., Formal, S.B., 1994. Epithelial cell penetration as an essential step in the pathogenesis of bacillary dysentery. J. Bacteriol. 43, 1503–1518.

Lario, P.I., Pfuetzner, R.A., Frey, E.A., Creagh, L., Haynes, C., Maurelli, A.T., Strynadka, N.C., 2005. Structure and biochemical analysis of a secretin pilot protein. EMBO J. 24, 1111–1121.

Magdalena, J., Hachani, A., Chamekh, M., Jouihri, N., Gounon, P., Blocker, A., Allaoui, A., 2002. Spa32 regulates a switch in substrate specificity of the type III secreton of *Shigella flexneri* from needle components to Ipa proteins. J. Bacteriol. 184, 3433–3441.

Marlovits, T.C., Kubori, T., Sukhan, A., Thomas, D.R., Galan, J.E., Unger, V.M., 2004. Structural insights into the assembly of the Type III secretion system needle complex. Science 306, 1040–1042.

Menard, R., Sansonetti, P.J., Parsot, C., 1993. Nonpolar mutagenesis of the Ipa genes defines *IpaB*, *IpaC*, and *IpaD* as effectors of *Shigella flexneri* entry into epithelial cells. J. Bacteriol. 175, 5899–5906.

Nouwen, N., Ranson, N., Saibil, H., Wolpensinger, B., Engel, A., Ghazi, A., Pugsley, A.P., 1999. Secretin PulD: association with pilot PulS, structure, and ion-conducting channel formation. Proc. Natl. Acad. Sci. 96, 8173–8177.

Oostergetel, G.T., Keegstra, W., Brisson, A., 1998. Automation of specimen selection and data acquisition for protein electron crystallography. Ultramicroscopy 74, 47–59.

Penczek, P., Radermacher, M., Frank, J., 1992. Three-dimensional reconstruction of single particles embedded in ice. Ultramicroscopy 40, 33–53.

Schuch, R., Maurelli, A.T., 1999. The Mxi-Spa type III secretory pathway of *Shigella flexneri* requires an outer membrane lipoprotein, *MxiM*, for invasin translocation. Infect. Immun. 67, 1982–1991.

Schuch, R., Maurelli, A.T., 2001. MxiM and MxiJ, base elements of the Mxi Spa type III secretion system of Shigella, interact with and stabilize the *MxiD* secretin in the cell envelope. J. Bacteriol. 183, 6991–6998.

Seydel, A., Gounon, P., Pugsley, A.P., 1999. Testing the +2 rule' for lipoprotein sorting in the Escherichia coli cell envelope with a new genetic selection. Mol. Microbiol. 34, 810–821.

Sosinsky, G.E., Francis, N.R., Stallmeyer, M.J., DeRosier, D.J., 1992. Substructure of the flagellar basal body of *Salmonella typhimurium*. J. Mol. Biol. 223, 171–184.

Sukhan, A., Kubori, T., Wilson, J., Galan, J.E., 2001. Genetic analysis of assembly of the *Salmonella enterica serovar typhimurium* type III secretion-associated needle complex. J. Bacteriol. 183, 1159–1167.

Sukhan, A., Kubori, T., Galan, J.E., 2003. Synthesis and localization of the *Salmonella* SPI-1 type III secretion needle complex proteins PrgI and PrgJ. J. Bacteriol. 185, 3480–3483.

Tamano, K., Aizawa, S., Katayama, E., Nonaka, T., Imajoh-Ohmi, S., Kuwae, A., Nagai, S., Sasakawa, C., 2000. Supramolecular structure of the *Shigella* type III secretion machinery: the needle part is changeable in length and essential for delivery of effectors. EMBO J. 19, 3876–3887.

Thomas, D., Morgan, D.G., DeRosier, D.J., 2001. Structures of bacterial flagellar motors from two FliF-FliG gene fusion mutants. J. Bacteriol. 183, 6404–6412.

Van Heel, M., 1984. Multivariate statistical classification of noisy images (randomly oriented biological macromolecules). Ultramicroscopy 13, 165–183.

Van Heel, M., 1987. Similarity measures between images. Ultramicroscopy 21, 95–100.

Van Heel, M., Schatz, M., Orlova, E., 1992. Correlation functions revisited. Ultramicroscopy 46, 307–316.

Yamaguchi, K., Yu, F., Inouye, M., 1998. A single amino acid determinant of the membrane localization of lipoproteins in *E. coli*. Cell 53, 423–432.

Yip, C.K., Kimbrough, T.G., Felise, H.B., Vuckovic, M., Thomas, N.A., Pfuetzner, R.A., Frey, E.A., Finlay, B.B., Miller, S.I., Strynadka, N.C.J., 2005. Structural characterization of the molecular platform for type III secretion system assembly. Nature 435, 702–707.

Yonekura, K., Maki-Yonekura, S., Namba, K., 2003. Complete atomic model of the bacterial flagellar filament by electron cryomicroscopy. Nature 424, 643–650.